Helicoids in chiral liquid crystals under external fields

G. De Matteis,[1,3,*] L. Martina,[1,2,†] C. Naya,[2,‡] and V. Turco[1,2,§]

[1]*Dipartimento di Matematica e Fisica, Università del Salento, Via Arnesano, 73100 Lecce, Italy*

[2]*INFN, Sezione di Lecce, Via Arnesano, Casella Postale 193I-73100 Lecce, Italy*

[3]*GNFM-INDAM, Città Universitaria, Piazzale Aldo Moro 5, Casella Postale 00185 Roma, Italy*

(Received 11 June 2019; revised manuscript received 6 August 2019; published 27 November 2019)

Cholesteric liquid crystals, subject to externally applied magnetic fields and confined between two parallel planar surfaces with strong homeotropic anchoring conditions, are found to undergo transitions to different types of helicoidal configurations with disclinations. Analytical and numerical studies are performed in order to characterize their properties. In particular, we produce a phase diagram for the transitions from the nematic state to the helicoidal phases in terms of the molecular chirality and the strength of the applied magnetic field.

DOI: 10.1103/PhysRevE.100.052703

I. INTRODUCTION

In the absence of external applied magnetic or electric fields and in free space, a cholesteric liquid crystal twists uniformly about a single axis: Rodlike chiral molecules self-assemble into a helical arrangement along a single direction. Under confinement, the natural twisted structures of the chiral nematic liquid crystals are often incommensurate with the geometry, dimension, and surface anchoring of the confining regions. Due to this geometric frustration, the confined chiral liquid crystals struggle to maintain their helical pitch and the preferred directors at the confining walls. A similar frustration mechanism takes place for a cholesteric liquid crystal in an electric or magnetic field: The field alignment is incompatible with the cholesteric twist. In both cases of frustration, the cholesteric is subject to an anisotropic environment: The competition between favored twist and anisotropy leads to the distortion and the partial or total unwinding of the helical nematic texture and to the formation of intriguing frustrated director configurations with topological defects [1,2]. The simultaneous interplay of the intrinsic molecular chirality, the external fields, and the boundary conditions, generate new structures either localized or extended. These structures can be elongated stringlike objects called *cholesteric fingers (or threads)* or *helicoids* [3–8], or they may be localized objects called *cholesteric bubbles* or *spherulitic domains* [9–12]. Recently, it has been recognized that cholesteric bubbles can have the remarkable properties of *skyrmions*. Skyrmions, originally proposed in the field of nuclear physics [13], are localized structures in which the magnitude of the order parameter (the nematic director **n** in this case) remains constant, but the orientation continuously varies in a complex texture that cannot be annealed away. Moreover, very recently, Smalyukh *et al.* generated in confined chiral liquid crystals a type of defects in the director field configurations, called *triple-twist torons*, by geometrical frustration and by using Laguerre-Gaussian vortex laser beams. They also showed numerically their existence from a theoretical point of view [14–16].

All such configurations, i.e., helicoids, skyrmions, torons, and other specific solitonic textures, e.g., *hopfions* and *merons* [14–17], are stabilized by some type of topological and/or nontopological conservation laws [18] and, at least, in some approximate setting, they can be described in terms of integrable nonlinear equations [19]. Moreover, these novel structures have been studied through a range of techniques, including experiments and numerical simulations in several confinement geometries, such as thin layers, wedge cells, cylindrical cavities, and spherical droplets [20–23]. Relevant variational and numerical calculations for skyrmions have been performed in two dimensions by Bogdanov and Shestakov [24] and Bogdanov *et al.* [25], and more recently in three dimensions by Leonov *et al.* [26]. In the latter paper, authors studied the Frank-Oseen (FO) free energy in the confined geometry,

$$\mathcal{B} = \left\{(x, y, z) \in \mathbb{R}^3, |z| \leqslant \frac{L}{2}\right\}, \tag{1}$$

L being the nematic cell gap under the action of an external field and with weak anchoring conditions, i.e., the Rapini-Popoular anchoring surface energy [27]. They calculated the director texture for skyrmions. The boundary conditions translate into conditions on the partial derivatives of the director on the confining surfaces. Later, in Ref. [28], the authors performed similar variational and numerical calculations in the same confining geometry but for the case of strong anchoring (**n** perpendicular at the confining surfaces) and in the absence of external fields. In particular, the authors of Ref. [28] worked out analytical and numerical solutions for a single helicoid and for a helicoid lattice. By using similar calculations, they investigated isolated skyrmions and skyrmion lattices.

In this paper, we consider a chiral liquid crystal confined within $\mathcal{B}$ as in (1) with strong homeotropic anchoring conditions and in the presence of an external magnetic field.

As opposed to Ref. [28], the inclusion of an external field leads to a nonlinear partial differential equation (PDE) for the

*giovanni.dematteis@istruzione.it
†martina@le.infn.it
‡carlos.naya@le.infn.it
§vito.turco@le.infn.it

director orientation angle, more precisely, the elliptic sine-Gordon equation on the strip, possibly with discontinuous boundary conditions. New static chiral states are found and recognized to be similar to cholesteric fingers (helicoids) with defects of disclination type [3,8]. We classify and describe these configurations by analytical and numerical methods. In particular, we discuss a new type of solutions called 2π helicoids where the director field $\mathbf{n}(\mathbf{r})$, independent of y, rotates by 2π over the strip, that is, the projection of $\mathcal{B}$ onto the (x, z) plane. In addition to the 2π helicoids, we also find π helicoids where the director $\mathbf{n}(\mathbf{r})$ only twists once over the strip. All these solutions contain disclination-type singularities. Accordingly, the evaluation of the static free energy leads to the introduction of a phenomenological cutoff, which, in turn, determines a critical parameter for the transition to the nematic uniform state. Transitions from the uniform nematic state to 2π and π helicoids are represented in the phase space of the spontaneous chiral twist and magnetic strengths.

The paper is organized as follows. In Sec. II, we introduce the mathematical model. In Secs. III and IV, we solve the nonlinear PDE problem and find the solutions in a closed analytical form. In Sec. V, we build up a phase diagram of the solutions by energy comparison. Finally, in Sec. VI, we draw our conclusions and plan future work.

II. THE MODEL

We consider a static cholesteric liquid crystal (CLC) layer, confined in between two identical planar surfaces placed at $z = \pm\frac{L}{2}$ and extending to infinity in the orthogonal directions (x, y) in a suitable Cartesian reference system (O, x, y, z) with orthonormal basis vectors $\mathbf{x}$, $\mathbf{y}$, and $\mathbf{z}$. The system is described by the unimodular director field $\mathbf{n}(\mathbf{r}) \in \mathbb{RP}^2$,

$$\mathbf{n}(\mathbf{r}) = [\sin\,\theta(\mathbf{r})\cos\,\phi(\mathbf{r}), \sin\,\theta(\mathbf{r})\sin\,\phi(\mathbf{r}), \cos\,\theta(\mathbf{r})], \quad (2)$$

due to the Z_2 symmetry of the microscopic model [29] and governed by the Frank-Oseen free energy density,

$$\mathcal{E}_{\mathrm{FO}} = \frac{K_1}{2}(\nabla\cdot\mathbf{n})^2 + \frac{K_2}{2}(\mathbf{n}\cdot\nabla\times\mathbf{n} - q_0)^2 + \frac{K_3}{2}(\mathbf{n}\times\nabla\times\mathbf{n})^2 - \frac{\chi_a}{2}(\mathbf{n}\cdot\mathbf{H})^2, \quad (3)$$

where q_0 is the spontaneous chirality constant of the cholesteric phase, whereas the positive reals K_i denote the splay, twist, and bend Frank elastic constants, respectively, for which we use the simplifying one constant approximation $K = K_1 = K_2 = K_3$. The last term represents the interaction energy density with an external static magnetic field $\mathbf{H} = H\mathbf{z}$, which is assumed to be uniform.

At the bounding surfaces, we impose strong homeotropic anchoring conditions, i.e., $\mathbf{n}(x, y, z = \pm\frac{L}{2}) = \mathbf{z}$.

Both $\mathbf{H}$ and the confinement break the general rotational and translational symmetries along the $\mathbf{z}$ direction of the fundamental cholesteric helices, i.e., $\mathbf{n}(\mathbf{r}) = (0, \sin\,q_0x, \cos\,q_0x)$. Hence, cholesteric helices are deformed, possibly leading to extended structures called helicoids or to localized cholesteric bubble domains, called spherulites, which have been considered in Refs. [19,30].

The special symmetry reduction (constant $\phi = -\pi/2$ and y invariance),

$$\mathbf{n}(\mathbf{r}) = [0, -\sin\,\theta(x, z), \cos\,\theta(x, z)] \quad (4)$$

for the director field leads to the cholesteric finger phase with its axis along the $\mathbf{x}$ direction and it simplifies the Frank-Oseen energy (3) to

$$E_{\mathrm{FO}-2d} = \frac{K}{2}\int_{-(L/2)}^{L/2} dz \int_{-\infty}^{\infty} dx \Big[[\partial_x\theta(x, z)]^2 + [\partial_z\theta(x, z)]^2 + 2q_0\partial_x\theta(x, z) + \frac{\chi_a H^2}{K}\sin^2\theta(x, z)\Big], \quad (5)$$

where the constant magnetic contribution of the nematic phase has been subtracted.

The corresponding equilibrium equation is the elliptic sine-Gordon,

$$\partial_x^2\Theta + \partial_z^2\Theta = \Lambda^2\sin\,\Theta, \quad \Theta = 2\theta, \quad \Lambda = \sqrt{\frac{\chi_a}{K}}H, \quad (6)$$

where Λ is the reciprocal of the magnetic coherence length. Please note that this equation does not depend on q_0 as the term $Kq_0\partial_x\theta$ in (5) is actually a null Lagrangian.

Large classes of solutions on the plane to Eq. (6) are well known in the literature [31] (and references therein), but here, we are dealing with different boundary conditions. Our reduction is the most natural extension of the problem considered in Ref. [28] and studied also in Ref. [32] in a linear setting. Here, we study the nonlinear problem. Strong homeotropic anchoring conditions require $\Theta(x, \pm\frac{L}{2}) = 2k\pi$ and $\Theta(x, \pm\frac{L}{2}) = 2k'\pi$ with $k, k' \in \mathbb{Z}$, for negative and positive x's, respectively. Thus, any nonconstant solution must have, at least, a jump singularity on the boundaries.

III. 2π HELICOIDS

In order to embody the above requirements, a known group-theoretical procedure [33] suggests a simple ansatz for the solution, corresponding to the form

$$\Theta = 4\,\arctan[X(x)Z(z)], \quad (7)$$

which separately depends on the x and z variables (see also Ref. [34]).

Plugging this expression into (6) and recalling the trigonometric identity $\sin(\arctan\,x) = \frac{x}{\sqrt{1+x^2}}$, we get

$$\frac{X''}{XZ^2} + X^2\left(\frac{Z''}{Z} - \frac{Z'^2}{Z^2}\right) = XX'' - 2X'^2 + \Lambda^2X^2 + \frac{Z''}{Z^3} - \frac{\Lambda^2}{Z^2}, \quad (8)$$

where $(\cdot)'$ and $(\cdot)''$ indicate the first and the second derivatives with respect to the argument, respectively.

The integration procedure of this equation is well known [34], but for self-consistency of the article and for convenience of the readers, we just sketch the main steps.

Then, performing the mixed derivative ∂_{xz}^2 to both sides of Eq. (8), the right hand side vanishes, and it becomes

$$2XX'\left[\frac{Z''}{Z} - \frac{Z'^2}{Z^2}\right]' - \frac{2Z'}{Z^3}\left[\frac{X''}{X}\right]' = 0. \quad (9)$$

The last equation can be separated in

$$\frac{1}{X'X}\left[\frac{X''}{X}\right]' = 4a, \tag{10}$$

$$\frac{Z^3}{Z'}\left[\frac{Z''}{Z} - 2\left(\frac{Z'}{Z}\right)^2\right]' = 4a, \tag{11}$$

where a is a separation constant.

Integrating Eqs. (10) and (11) with respect to x and z, one obtains

$$X'' = 2aX^3 + bX, \tag{12}$$

$$\frac{Z''}{Z} - 2\left(\frac{Z'}{Z}\right)^2 + \frac{2a}{Z^2} + d = 0, \tag{13}$$

which can be further integrated [i.e., multiplying the equation for $Z(z)$ in (13) by (Z'/Z^3)] to get

$$(X')^2 = aX^4 + bX^2 + c, \tag{14}$$

$$(Z')^2 = gZ^4 + dZ^2 + a. \tag{15}$$

Equations (14) and (15) contain five constants (the separation constant a and the integration constants b, c, d, and g), but only three of them are independent. Indeed, substituting them in Eq. (8), one can easily obtain the relations,

$$g = c, \quad b = \Lambda^2 - d.$$

Thus, Eqs. (14) and (15) can be written in the final form

$$(X')^2 = aX^4 + (\Lambda^2 - d)X^2 + c, \tag{16}$$

$$(Z')^2 = cZ^4 + dZ^2 + a, \tag{17}$$

which are solvable in terms of Jacobi elliptic functions.

The steplike conditions on the boundaries force to have $Z(\pm\frac{L}{2}) = 0$ and to look for functions $X(x)$ monotonic and unbounded also at some finite point. Then, one obtains

$$X(x) = \pm\sqrt{\frac{\Lambda^2 - d}{a}}\,\mathrm{csch}(\sqrt{\Lambda^2 - d}x), \tag{18}$$

where $a > 0$ and $\Lambda^2 > d$.

As for $Z(z)$, the compatibility of Eq. (17) with the sine-Gordon (6) and the above boundary conditions set $d = -\frac{\pi^2}{L^2}$ in order to have real θ with the semiperiod of the corresponding $Z(z)$ exactly equal to the thickness L of the sample. Thus, we are led to the general expression,

$$\theta_n = 2\,\arctan\left[\frac{c_n\ell}{\pi(1+2n)}\frac{\cos\left(\frac{\pi(1+2n)z}{L}\right)}{\sinh\left(c_n\ell\frac{x}{L}\right)}\right] - \pi\,\mathrm{sgn}\,x \tag{19}$$

for $n \in \mathbb{N}$ and where the effective scale $\ell = \Lambda L$ and the modal factor $c_n = [1 + \frac{(1+2n)^2\pi^2}{\ell^2}]^{1/2}$ have been introduced. The asymptotic behavior of this family of solutions is $\theta \overset{x\to\pm\infty}{\longrightarrow} \mp\pi$, that is, the director field $\mathbf{n}(\mathbf{r})$ rotates by 2π over the strip as depicted in Fig. 1.

We first observe that the solution only depends on the structural parameters L and Λ via their product ℓ. Second, there exists an entire spectrum of excitations indexed by $n \geqslant 0$. Since, for $n > 0$, solutions are discontinuous at $x = 0$ and $\cos[\pi(1+2n)z/L] \leqslant 0$, the most physically meaningful solution corresponds to $\theta_0(x, z)$ (Fig. 1), which is continuous and differentiable at all points of the strip but at the special points $(x = 0,\ z = \pm\frac{L}{2})$. Here, it exhibits a discontinuity of 2π, indicating the presence of a disclination along the $\mathbf{y}$ direction.

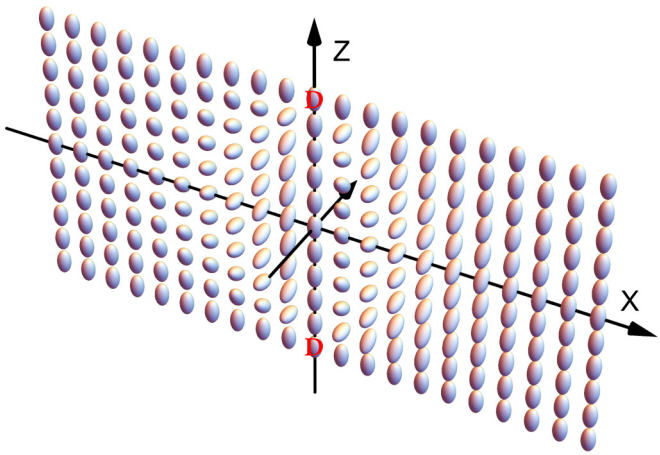

FIG. 1. Distribution of $\mathbf{n}(\mathbf{r})$ for the 2π helicoid, given in (19) for $n = 0$. The picture shows a cross section of the configuration at $y = 0$ for $\Lambda L = 1$. The disclination is indicated by the letter D.

Whereas the dependency on z is determined uniquely by L, on the x variable, the typical scale is $\Lambda^{-1}(1 + \frac{\pi^2}{\ell^2})^{-(1/2)}$, which comes from the tendency of the external magnetic field to align the molecules along its direction, further enhanced by the anchoring of the bounding surfaces.

We also note that solution (19) can be obtained by applying the nonlinear Bianchi superposition formula [35] for two one-kink solutions of the elliptic sine-Gordon (6). Such a theorem states that if Θ, Θ_1, and Θ_2 are three solutions related by the overdetermined first order system, the so-called Bäcklund transformation,

$$(\partial_x - \imath\,\partial_y)\left(\frac{\Theta_i - \Theta}{2}\right) = \beta_i\Lambda\,\sin\left(\frac{\Theta_i + \Theta}{2}\right), \tag{20}$$

$$(\partial_x + \imath\,\partial_y)\left(\frac{\Theta_i + \Theta}{2}\right) = \frac{\Lambda}{\beta_i}\sin\left(\frac{\Theta_i - \Theta}{2}\right), \tag{21}$$

$(\beta_i \in \mathbb{C},\ i = 1, 2)$, then a fourth solution is given by

$$\bar{\Theta} = \Theta + 4\,\arctan\left[\frac{\beta_2 + \beta_1}{\beta_2 - \beta_1}\tan\left(\frac{\Theta_2 - \Theta_1}{4}\right)\right]. \tag{22}$$

As an application, one solves the system (20) and (21) corresponding to the trivial solution $\Theta = 0$. This leads to the kink solutions $\Theta_i = 4\,\arctan\,[\exp\,(a_i + \frac{\beta_i\Lambda\zeta}{2} + \frac{\Lambda\bar{\zeta}}{2\beta_i})]$ with a_i integration constants for $i = 1, 2$. Combining these two expressions into formula (22) and requiring real solutions for real variables, one is led to the constraints $\beta_2 = \beta_1^{-1}$ and $a_1 = 0$, $a_2 = \imath\pi$. Furthermore, imposing the boundary condition, one arrives at the expression (19) with $\beta_1 = c_n + \sqrt{c_n^2 - 1}$.

This result suggests that multiple 2π-helicoid solutions may be built up by iterating the process. Unfortunately, the boundary conditions we impose are too rigid, and they lead to singular solutions, which will be excluded from further discussions.

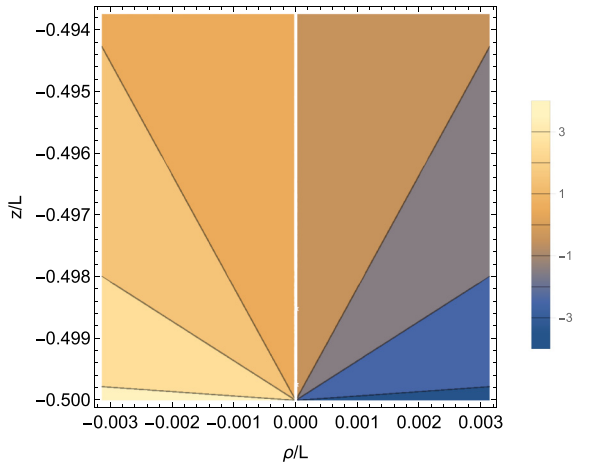

FIG. 2. Contour plot of θ_0 around the disclination located at $x = 0,\ z = -L/2$.

Finally, let us observe that since the total change in θ is 2π, we can distinguish two regions where the director rapidly passes through $\frac{\pi}{2}$, sandwiched by three different regions in which the liquid crystal is close to the uniform state. Around the disclination, θ_0 has a conformally invariant behavior which, in cylindrical coordinates $x = \rho\cos t,\ z = -\frac{L}{2} + \rho\sin t$, can be expressed as a series with respect to ρ, namely,

$$\theta_0 = -\pi\,\mathrm{sgn}(\cos t) + 2t - \frac{\sin(2t)(\ell^2\cos^2 t + \pi^2)}{6}\left(\frac{\rho}{L}\right)^2 + O\left[\left(\frac{\rho}{L}\right)^4\right], \quad 0 \leqslant t \leqslant \pi. \tag{23}$$

Thus, θ_0 is almost independent of the distance ρ from the disclination as shown by the contour plot in Fig. 2. The corresponding singularity in the energy signals a loss of order, and, therefore, physically, in the vicinity of the disclination, the liquid crystal is melted from the ordered to the disordered isotropic phase. To avoid the singularity, we single out a small semidisk of radius $a \ll \frac{L}{2}$ around the disclination and replace it with a region in the isotropic phase where it is common practice to uniformly impose an energy density cutoff $\mathcal{E}_{\max} \approx \frac{K}{a^2}$ with $a \approx 10^{-2}$–$10^{-3}L$ [32].

By using analytical solution (19), we can write down an expression for the difference of energy with respect to the nematic phase in the limit of small a/L, which, up to second order, reads

$$\Delta E_{2\pi} = E_{2\pi} - E_{\mathrm{nem}} \approx \frac{K}{3}\left\{24G + 10a^2\Lambda^2 + 12\sqrt{\pi^2 + \Lambda^2L^2} + 3aq_0\ln(16) - 2\pi\left[6 - 3aq_0 + 3Lq_0 + 2a^2\Lambda^2 + 6\ln\left(\frac{a}{2L}\right) + 3\ln[\Lambda^2L^2 + 2\pi(\pi + \sqrt{\pi^2 + \Lambda^2L^2})]\right]\right\}, \tag{24}$$

where G is the Catalan constant. Please note that $E_{2\pi}$ corresponds to the energy of the 2π helicoids whereas E_{nem} stands for the energy of the nematic phase, which equals zero as can be seen from Eq. (5).

At thermal equilibrium, stable 2π helicoids may exist if $\Delta E_{2\pi} < 0$; from the latter condition, one can infer a critical transition value for the chiral twist parameter as a function of the external field Λ. Note that, due to the presence of the external field, expansion (24) for small a/L holds as far as ΛL is not very high, which is true in the range of interest. By neglecting the $(a/L)^2$ contributions in (24) and introducing the cutoff energy, we arrive at

$$\Delta E_{2\pi} = 2KL(q_H - q_0)\left(\pi - \frac{1}{L}\sqrt{\frac{K}{\mathcal{E}_{\max}}}[\pi + \ln(4)]\right), \tag{25}$$

with

$$q_H = \frac{4G - 2\pi + 2\sqrt{\pi^2 + \Lambda^2L^2} + \pi\,\ln\left(4L^2\frac{\mathcal{E}_{\max}}{K}\right) - \pi\,\ln[\Lambda^2L^2 + 2\pi(\pi + \sqrt{\pi^2 + \Lambda^2L^2})]}{L\left(\pi - \frac{1}{L}\sqrt{\frac{K}{\mathcal{E}_{\max}}}[\pi + \ln(4)]\right)}, \tag{26}$$

the critical chiral twist. Since the disclination radius has an important effect in locating the phase transition, q_H might be used to estimate the effective size of the defects appearing in real liquid crystal samples.

IV. π HELICOIDS

In a "more elementary" class of helicoids the director $\mathbf{n}(\boldsymbol{r})$ twists only once when going from the vacuum state $\theta = \pi$ at $x \to -\infty$ to the nearest $\mathbb{Z}_2$ equivalent one, namely, $\theta = 0$ for $x \to +\infty$. Moreover, because of the homeotropic anchoring, the boundary conditions on the confining surfaces will be

$$\theta\left(x, z = \pm\frac{L}{2}\right) = \begin{cases}\pi, & x < 0,\\ 0, & x > 0.\end{cases} \tag{27}$$

Then, in such a kind of solutions, which we call π helicoids, a couple of disclinations appear on the boundaries, parallel to the y axis. The analysis of the full nonlinear problem (6) with boundary values (27) is quite involved, even if one would profit from the integrability properties of the sine-Gordon equation through its Lax pair formulation as developed in Ref. [36] and references therein (see the Appendix for more details). Actually, the Lax pair problem is a matrix linear

representation of the overdetemined Bäcklund system (20) and (21), and it is equivalent to finding a matrix integration factor $\Psi(x, z; \lambda)$, depending on an auxiliary complex parameter λ, which makes the following one-form exact

$$W = \exp\left[\Omega(\lambda)x + \omega(\lambda)z\frac{\hat{\sigma}_3}{2}\right][Q(x,z,\lambda)\Psi\, dx + \imath Q(x,z,-\lambda)\Psi\, dz]$$
$$= d\left[\exp\left(\Omega(\lambda)x + \omega(\lambda)z\frac{\hat{\sigma}_3}{2}\right)\Psi\right], \tag{28}$$

with $\hat{\sigma}_3 \cdot = [\sigma_3, \cdot]$, σ_i being the Pauli matrices, $\Omega(\lambda)$ and $\omega(\lambda)$ the dispersion functions on $\mathbb{C}_\lambda/\{0\}$ defined as

$$\Omega(\lambda) = \frac{\imath\Lambda}{2}\left(\frac{1}{\lambda} - \lambda\right), \quad \omega(\lambda) = \frac{\Lambda}{2}\left(\frac{1}{\lambda} + \lambda\right), \tag{29}$$

and $Q(x, z, \lambda)$ as the *potential* matrix,

$$Q(x,z,\lambda) = \frac{\imath}{4}\left(\frac{\Lambda}{\lambda}(1 - \cos\,\Theta)\sigma_3 + (\Theta_x - \imath\Theta_z)\sigma_1 - \frac{\Lambda}{\lambda}\sin\,\Theta\sigma_2\right). \tag{30}$$

Then, one can check that the closure condition of W implies that Θ has to satisfy the sine-Gordon equation (6). However, this type of construction also requires the knowledge of the derivatives normal to the boundaries, possibly containing singularities not included in (27). These difficulties are not alleviated in the limit of the linear approximation, which can be obtained by letting $\Theta = 2\theta \approx 0$ and $\Psi \approx \mathbf{1}_2$, namely,

$$W_{\text{lin}} = 2e^{-\Omega(\lambda)x - \omega(\lambda)z}\left[\imath\left(\theta_x - \imath\theta_z - \frac{\Lambda\theta}{\lambda}\right)dx - \left(\theta_x - \imath\theta_z + \frac{\Lambda\theta}{\lambda}\right)dy\right]. \tag{31}$$

To avoid such an addition of extra information about the derivatives, a long procedure was introduced in Ref. [37]. Such work led to a unifying approach in solving both linear and nonlinear boundary value problems via a suitable integral mapping of the boundary data into the solution [38].

The closure condition of W_{lin} yields the modified Helmholtz equation which can be solved by different types of transform methods, thus, bypassing the above mentioned problem of the derivatives on the boundary. By exploiting the discrete mirror symmetry along the x axes of our problems (6) and (27), the modified Helmholtz boundary value problem on the semistrip arises

$$\partial_x^2\theta_+ + \partial_z^2\theta_+ = \Lambda^2\theta_+ \;\forall\, x > 0, \tag{32a}$$

$$\theta_+\left(x, z = \frac{\pm L}{2}\right) = 0, \quad \theta_+(x = 0^+, z) = \frac{\pi}{2} \;\forall\, |z| < \frac{L}{2},$$
$$\theta_-(x,z) = \pi - \theta_+(-x,z), \;\forall\, x < 0 \text{ and } |z| < \frac{L}{2}. \tag{32b}$$

In principle, this system could be solved by standard Fourier series methods [39]. Because of the linearity of the equation and the separability of the independent variables, one can look for solutions of (32) in the form $\theta_+(x,z) = \sum_{k=0}^{\infty} X_k(x)Z_k(z)$, where Z_k belongs to an orthonormal basis of the $L^2_{[-(L/2),+(L/2)]}$ space. Taking into account the vanishing of the series at $|z| = \frac{L}{2}$, one sets $Z_k = \sqrt{\frac{2}{L}}\cos\left(\frac{\pi(2k+1)z}{L}\right)$. Assuming that the series is absolutely and uniformly convergent together with its derivatives, its substitution into (32) can be computed by exchanging the sum with the Laplacian operator, which will act term by term. Using the orthonormalization of Z_k for the generic coefficient, one gets the equation,

$$X_k'' = \left[\Lambda^2 + \left(\frac{\pi(2k+1)}{L}\right)^2\right]X_k. \tag{33}$$

The corresponding solutions are real exponentials from which we only keep those vanishing as x tends to infinity, namely, $X_k = \xi_k \exp\left[-\frac{x\sqrt{\pi^2(2k+1)^2 + \Lambda^2L^2}}{L}\right]$. The amplitudes ξ_k are simply determined by letting $x \to 0$ and using again the orthonormalization of Z_k for the series $\sum_{k=0}^{\infty}\xi_k Z_k = \frac{\pi}{2}$, we are led to the solution,

$$\theta_+(x,z) = 2\sum_{k=0}^{+\infty}\frac{(-1)^k}{2k+1}\exp\left[-\frac{x\sqrt{\pi^2(2k+1)^2 + \ell^2}}{L}\right]$$
$$\times\cos\left(\frac{\pi(2k+1)z}{L}\right). \tag{34}$$

This latter cannot be cast in a factorized form as in (19) unless when $\Lambda = 0$. In this case, the series can be summed up to the closed form

$$\theta_+(x,z) = \arctan\left[\frac{\cos\left(\frac{\pi z}{L}\right)}{\sinh\left(\frac{\pi x}{L}\right)}\right], \tag{35}$$

which, upon using the trigonometric identity $\arctan u + \arctan v = \arctan\left(\frac{u+v}{1-uv}\right)$, matches Eq. (10) in Ref. [28] up to a global sign due to the equivalence $\theta \to \pi - \theta$ in order to comply with their far-field values.

Using expression (32b), one can continuously complete the solution also for $x < 0$ except at the points $(x = 0,\ z = \pm\frac{L}{2})$. The exponential decaying in x has the characteristic length $\Delta x \approx \frac{2L}{\sqrt{\ell^2+\pi^2}}$.

However, close to $x = 0$, the linear approximation to the sine-Gordon might be unsatisfactory, first because $\sin\frac{\pi}{2} \neq \frac{\pi}{2}$,

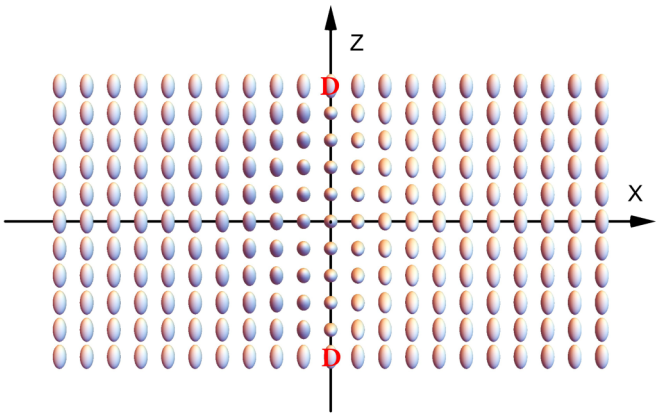

FIG. 3. Distribution of the $\mathbf{n}(x, z)$ field for the π helicoid. The picture shows a cross section of the configuration at $y = 0$ for $\Lambda L = 1$. The disclination is indicated by the letter D.

and second because there the series (34) is not uniformly and absolutely convergent, implying all well known convergence problems at the discontinuity points. Moreover, the partial derivatives $\partial_x\theta(x, z)$ and $\partial_z\theta(x, z)$ are diverging for $x \to 0^{\pm}$ and $z \to \pm\frac{L}{2}$. So the differentiability of θ on the segment $\{x = 0,\ |z| < L/2\}$ is lost.

By finding an integration factor associated with the one-form W_{lin} in Eq. (31), we can also adopt a different representation of the same solution (see the Appendix for details) as follows [40]:

$$\theta_+(x, z) = \frac{-1}{2\pi}\left[\int_{-\infty}^{0} e^{\Omega(\lambda)x+\omega(\lambda)[z+(L/2)]}G_1(\lambda)\frac{d\lambda}{\lambda} + \int_{\infty}^{0} e^{\Omega(\lambda)x+\omega(\lambda)[z-(L/2)]}G_1(\lambda)\frac{d\lambda}{\lambda} + \int_{0}^{-\imath\infty} e^{\Omega(\lambda)x+\omega(\lambda)[z+(L/2)]}G_2(\lambda)\frac{d\lambda}{\lambda}\right], \quad (36)$$

where

$$G_1(\lambda) = \frac{\imath\pi}{4}\frac{1-\lambda^2}{1+\lambda^2}\frac{e^{\omega(\lambda)L}-1}{e^{\omega(\lambda)L}+1}, \quad (37)$$

$$G_2(\lambda) = \frac{\imath\pi}{4}\frac{1-\lambda^2}{1+\lambda^2}(1-e^{-\omega(\lambda)L}) \quad (38)$$

encode the information about the boundary conditions. In particular, the function $G_1(\lambda)$ has the poles ($\ell = \Lambda L$),

$$P_G = \{-\imath[\sqrt{\ell^2+(2n+1)^2\pi^2}-\pi(2n+1)]/L\}_{n\in\mathbb{Z}}. \quad (39)$$

As expected, the corresponding residues lead to expansion (34), this bringing both approaches together. On the other hand, by looking at the analytic properties of the integrands in the lower half-plane $\mathbb{C}_\lambda$, one may suitably deform the integration contour in formula (36) in order to extract more information about the solution near the singularities. This alternative approach might be the starting point to study the full nonlinear problem, which still presents difficulties to get an explicit formula [37] (in particular, the singular behavior of the solution around the disclination).

In Fig. 3, $\mathbf{n}(x, z)$ is represented by using formula (34) up to $k = 10$. At $(0, \pm\frac{L}{2})$, an overlap of directional ellipsoids occurs, thus, giving rise to disclinations extended in the orthogonal direction y. However, the actual configuration is sensitive to the involved parameters, which control also how good the linear approximation is. To have more insight in the π helicoids, a numerical boundary value problem solver has been implemented for the full nonlinear system. We employed standard numerical techniques, namely, the central finite difference scheme accompanied by appropriate application of Newton's iterative method for the calculation of the function $\theta(x, z)$ over a suitable grid [41,42]. The problem can be coded in almost any programming language. However, we used MATLAB© by Mathworks [43] because of the natural way it operates with large and sparse matrices.

In Fig. 4, a comparison between the numerical solutions and the analytical series up to 7000 terms is presented. Although the similarity of the profiles is remarkable at this accuracy, a study of the Laplacians shows the expected differences associated with the different equations solved (either modified Helmholtz or sine-Gordon).

V. PHASE TRANSITION DIAGRAM

In order to assess the relative stability of the solutions, we have found above, i.e., π and 2π helicoids, we need now to perform an energy analysis and to compare the solutions also with the uniform nematic configurations to see which one is energetically favored in terms of the physical parameters involved, namely, q_0 and Λ. To this purpose, we use solutions (19) for $n = 0$ and (34) with its extension for negative x where, in the latter, we truncated the series at $k_{\text{max}} = 7000$.

Recalling that the chiral strength q_0 is a function of the temperature (linear under certain conditions), one could interpret the phase diagram as the result of thermal-magnetic competitive effects in the formation of the helicoids. When the energy of both solutions is greater than zero, the homeotropic nematic phase is the favored one. It is important to note that the transitions between the three different configurations occur along two different curves (see Fig. 5). There are two different thresholds in chirality strength for a fixed magnetic field also depending on the disclination size a/L. In Fig. 5, we have set $a/L = 10^{-2}$, although, for smaller values of a/L, the shape of the diagram does not change. In particular, if a study of a pair of π helicoids as a function of the distance between them is realized, one can see the energy increasing when they approach. This implies the existence of a barrier preventing the two helicoids from sitting on top of each other unless some energy is introduced into the system from outside. This underlines the stability of the 2π helicoids with disclinations located at the boundaries with respect to the decay into two π helicoids with disclinations placed at the same point, which correspond to completely different configurations. Conversely, this is not the case when $\Lambda = 0$ where the two configurations are equivalent.

Moreover, the curve between the nematic and the π-helicoid phases should be the analogous of the straight line $\Lambda_0 = \frac{\pi|q_0|}{2}$ in the bulk model [44]. Deviations from such a behavior are related to the anchoring, possibly leading to significant variations in the value of the critical external field. Moreover, in Ref. [32], a semiempirical coexistence curve between the homeotropic and the cholesteric phases was

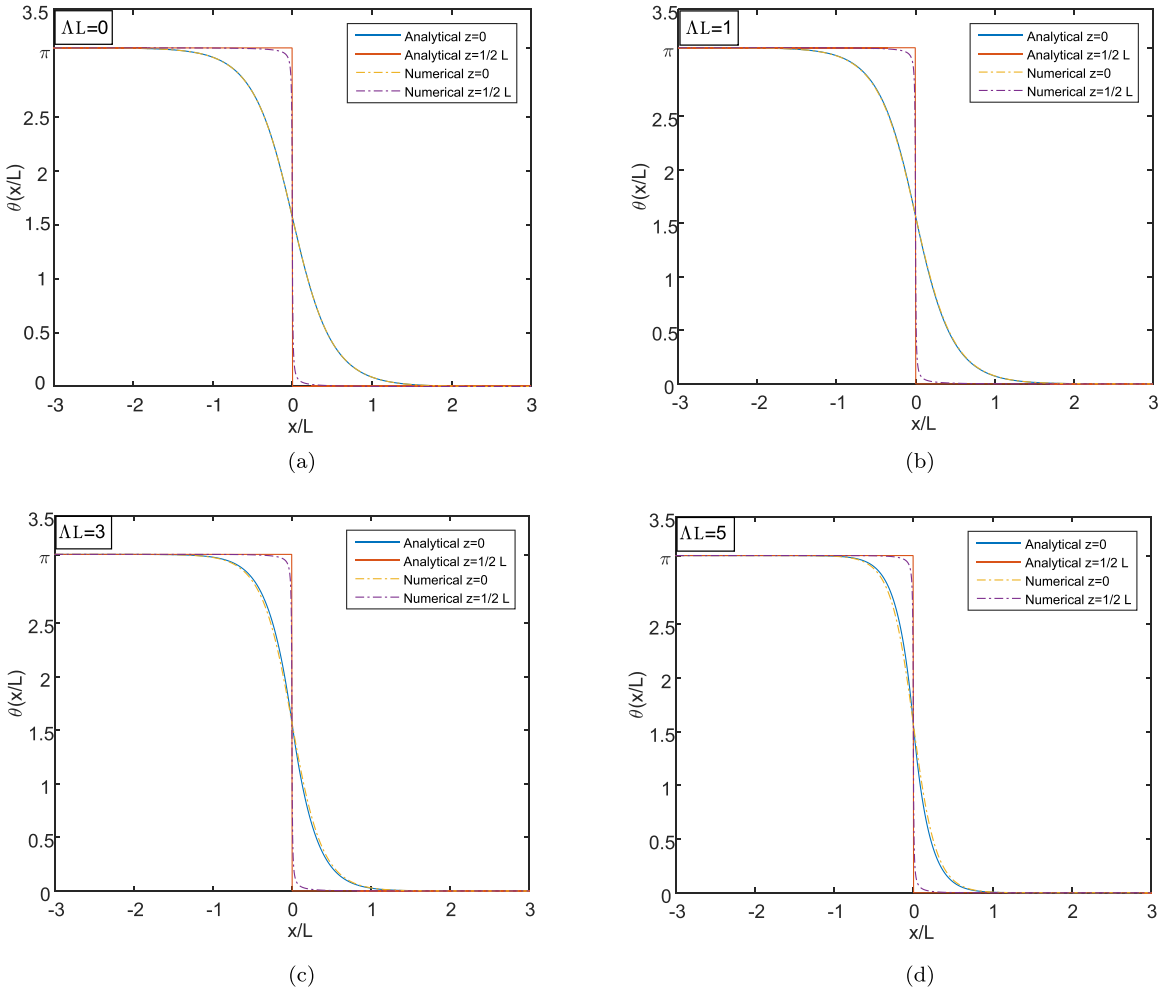

FIG. 4. Comparison of the numerical and approximated π-helicoid solutions for different values of the external field: (a) $\Lambda L = 0$, (b) $\Lambda L = 1$, (c) $\Lambda L = 3$, and (d) $\Lambda L = 5$

found, providing the critical external field $\Lambda_c L$ in terms of the cholesteric twist $q_0 L$. Using the present notation, such a relation reads

$$\Lambda_c L = \sqrt{\frac{2\gamma^2 qL\left(qL - \frac{2}{\gamma}\right)}{1 - \frac{(1-e^{-\gamma qL})}{\gamma qL}}}, \tag{40}$$

with $\gamma = K_2/K$ and

$$qL = -\frac{1}{\gamma} W_{-1}\left(-\frac{\gamma L}{2a} e^{-1-q_0 L\gamma}\right), \tag{41}$$

where W_k is the kth branch of the Lambert W function [45]. A fitting procedure to our numerical data leads to $\gamma = 1.054$, in excellent agreement with our assumed one constant approximation (i.e., $\gamma = 1$). The corresponding best fit curve is displayed in Fig. 5 (black dashed line).

VI. CONCLUSIONS

Summarizing, we have analytically found 2π helicoids which are configurations in bounded CLCs with homeotropic anchoring, allowed by the nonlinearity arising from the presence of an external field. Analogously, we studied a different type of helicoids, the π ones. If the former configuration can be derived in a closed form, for instance, by the Bäcklund transformations, for the latter, we have obtained approximated expressions and numerical solutions. Both classes of configurations are characterized by the presence of disclinations, located at the boundaries. The disclinations imply energy density divergences, which may be overcome by introducing a phenomenological energy cutoff, corresponding to excluded regions of melted crystal.

Numerically, we provided a phase diagram in the parameters $q_0 L$ and ΛL, which established the energetically favored configurations among them, the uniform nematic phase, and the corresponding transitions. We showed that π helicoids switch to 2π helicoids under certain circumstances dictated by the parameters of the problem. In particular, for a fixed value of the external field, we found the sequence uniform-to-π-to-2π helicoids as the value of the chirality increases as expected.

We would like to specify that other configurations, such as the three-dimensional objects discussed in the Introduction and helicoid lattices, might modify the phase diagram presented in Fig. 5. However, it is not necessary to introduce them in order to characterize the cholesteric-nematic transition we

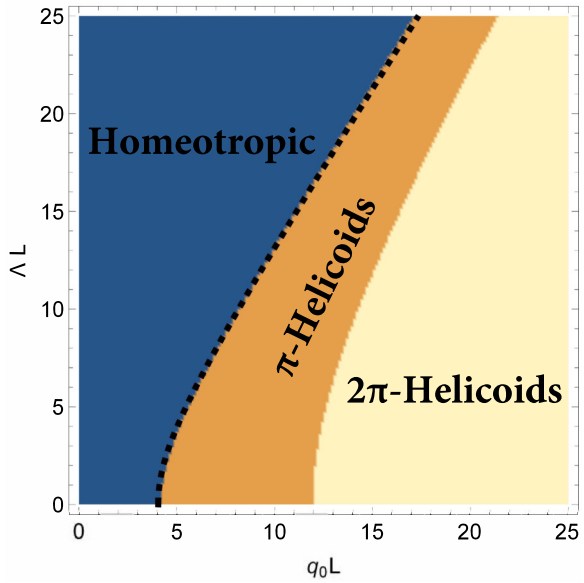

FIG. 5. Phase diagram on the plane $Lq_0, L\Lambda$, representing the nematic (blue), π-helicoid (orange) and 2π-helicoid (ochre) phases. The dashed black line corresponds to the best fit to (40).

found as shown by the agreement of our results with those obtained in Ref. [32] and the nature of the disclinations at the boundaries. This approach is similar to previous studies of analytical solutions limited to single helicoids with disclinations but in the absence of external fields and under the assumption of y invariance (see, for instance, Refs. [46,47] and [28,48]). Preceding detailed energy computations are now extended to the case of external fields in order to draw a theoretical phase diagram which can be considered equivalent to the experimental or semiempirical ones presented in Refs. [5,32,49].

This paper provides a step forward in the analytical construction of the fully comprehensive phase transition diagram for geometrically frustrated chiral nematics, which, to the best of our knowledge, is still a crucial and formidable problem for liquid crystals theory. In this spirit, the next step to be taken would be the study of the existence of lattices of helicoids, their interactions, and the corresponding phase diagram.

ACKNOWLEDGMENTS

The authors are thankful to the referees for their comments and suggestions. C.N. was supported by the INFN Grant No. 19292/2017 *Integrable Models and Their Applications to Classical and Quantum Problems*. L.M. has been partly supported by INFN through the MMNLP project by CSN4.

APPENDIX

In this Appendix, we give details about the derivation of the integral solution (36) to the modified Helmoltz boundary value problem and its relation to the series representation (34).

The sine-Gordon Eq. (6) is well known to be solvable via the inverse spectral transform (IST) [36] for initial data given at a fixed value of one of the independent variables. The IST is an integration procedure, which consists of studying the analytical properties of the wave functions of a specific linear differential operator (sometimes called the principal Lax operator) in one independent variable. Then, analytical deformations in the other independent variable of those wave functions are obtained by the action of a second suitable differential linear operator. In our case, these operators, called a Lax pair, possess the key property to have the sine-Gordon as their compatibility (commutativity) condition. This formulation introduces a complex spectral parameter λ, analogous to the momentum and frequency in the Fourier transform method. In fact, one may encode information of the solution (such as initial data and/or boundary values) into certain specific functions of λ: the so-called scattering data. The second Lax operator leads to linear differential equations determining the deformations of the scattering data. These new data are used to reconstruct the solution of the sine-Gordon for any value of the pair of independent variables by solving the so-called inverse linear spectral problem. Moreover, the scattering data are determined by the singularities of the principal Lax operator wave functions on the complex λ plane. Under suitable asymptotic assumptions on the sine-Gordon solutions, independent wave functions are sectionally holomorphic on the λ plane and the corresponding jump functions along the curves separating the holomorphicity regions provide the scattering data. Now, in classical complex function theory, solving the Riemann-Hilbert problem means reconstructing these sectionally holomorphic wave functions from given jump functions [50]. This is an equivalent way to formulate the inverse spectral problem. This idea can be readily applied also in the elliptic case with rather general boundary conditions, provided that suitable jump functions are assured [38,51]. For the sine-Gordon on the semistrip, this approach was almost fully developed in Ref. [37] (and references therein) where a unified method both for linear and for nonlinear integrable equations has been developed. Thus, this includes the treatment of the linear (modified) Helmholtz equation, which is exactly the linear approximation to our original model (6). Thus, in the present Appendix, we will apply such methods to extract interesting information in the linear case given by Eq. (32a). This simplification is supported by numerical calculations (see the discussion at the end of Sec. IV). In fact, it turns out that linear and nonlinear treatments show quite small differences in the quantitative behavior of the solutions near the disclination and for values of $\theta \approx \frac{\pi}{2}$ where we are far from a linear scheme.

As mentioned in the main text, in the unified approach to the study of the sine-Gordon and the modified Helmholtz equations, the traditional Lax pair formulation is equivalent to finding a matrix integration factor $\Psi(x, z; \lambda)$ (the wave function), depending on λ, which makes the one-form W in Eq. (28) exact.

The first observation is that W_{lin} in Eq. (31) remains closed by adding a suitable exact one-form $d[e^{\Omega x+\omega z}\kappa(x, z)]$. In particular, one can choose the function $\kappa(x, z)$ in such a way to cancel the $\partial_z\theta$ ($\partial_x\theta$) terms from the dx (dz) component.

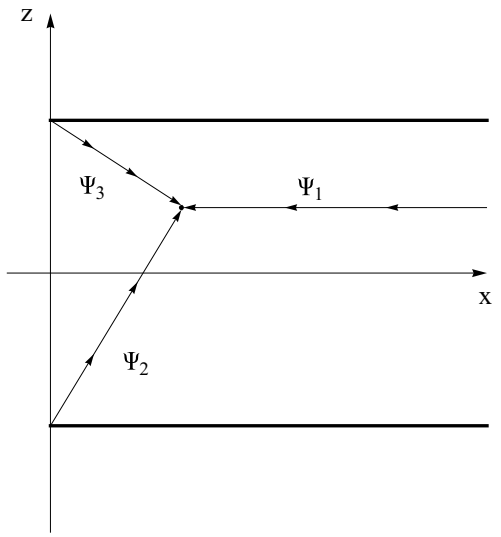

FIG. 6. Integration path for the Riemann-Hilbert problem (A4)–(A6).

A special case is given by

$$W_{\rm lin}^{\rm mod} = \frac{e^{-\Omega(\lambda)x-\omega(\lambda)z}}{2} \times \left[\left(\imath\theta_x - \Omega(\lambda)\int_x^{+\infty}\theta_z(\xi,z)d\xi + \frac{\Lambda\theta}{\lambda}\right)dx + \left(\imath\theta_z - \frac{\imath\Lambda\theta}{\lambda} + \int_x^{+\infty}\theta(\xi,z)d\xi - \omega(\lambda)\int_x^{+\infty}\theta_z(\xi,z)d\xi\right)dz\right], \tag{A1}$$

where Ω and ω are as in Eq. (29).

Suppose now that the boundary corresponds to a semistrip where the value for θ is assigned on its three sides. Then, in analogy with Eq. (28), we look for three functions Ψ_j, $j = 1$–3 such that

$$d(e^{-\Omega(\lambda)x-\omega(\lambda)z}\Psi_j) = W_{\rm lin}^{\rm mod}. \tag{A2}$$

By integrating along the paths shown in Fig. 6 (as many as the sides of the semistrip) with the initial conditions,

$$\Psi_1(+\infty,z;\lambda) = \Psi_2\left(0,-\frac{L}{2};\lambda\right) = \Psi_3\left(0,\frac{L}{2};\lambda\right) = 0 \tag{A3}$$

for any λ, one finds the functions Ψ_j, which are related by

$$\Psi_3 - \Psi_1 = -e^{\Omega x+\omega z}e^{-\omega(L/2)}\Psi_1\left(0,\frac{L}{2};\lambda\right), \tag{A4}$$

$$\Psi_3 - \Psi_2 = e^{\Omega x+\omega z}e^{\omega(L/2)}\Psi_3\left(0,-\frac{L}{2};\lambda\right), \tag{A5}$$

$$\Psi_1 - \Psi_2 = e^{\Omega x+\omega z}e^{\omega(L/2)}\Psi_1\left(0,-\frac{L}{2};\lambda\right). \tag{A6}$$

The consistency of these equations requires the global condition,

$$e^{-\omega L}\Psi_1\left(0,\frac{L}{2};\lambda\right) - \Psi_1\left(0,-\frac{L}{2};\lambda\right) + \Psi_3\left(0,-\frac{L}{2};\lambda\right) = 0. \tag{A7}$$

If the analyticity properties of the functions Ψ_j are determined and the right hand side of (A4)–(A6) are known, such a system will define a Riemann-Hilbert problem associated with the original modified Helmholtz boundary value problem (BVP).

Proceeding in this way, one first integrates Eq. (A2) along path 1, obtaining

$$\Psi_1 = -\frac{1}{2}\int_x^{\infty} e^{\Omega(x-x')}\left[\imath\theta_{x'} + \frac{\Lambda\theta}{\lambda} - \Omega(\lambda)\int_{x'}^{+\infty}\theta_z(\xi,z)d\xi\right]dx'. \tag{A8}$$

Hence, the constants appearing in (A4) and (A6) are given by

$$\Psi_1\left(0,\pm\frac{L}{2};\lambda\right) = -\frac{1}{2}\int_0^{\infty} e^{-\Omega x'}\left[\imath\theta_{x'}\left(x',\pm\frac{L}{2}\right) + \frac{\Lambda\theta\left(x',\pm\frac{L}{2}\right)}{\lambda} - \Omega(\lambda)\int_{x'}^{+\infty}\theta_z\left(\xi,\pm\frac{L}{2}\right)d\xi\right]dx'. \tag{A9}$$

Since $x' \geqslant 0$, the above integrals are convergent for $\Im\lambda > 0$.

Now, in (A5) the quantity $\Psi_3(0,-\frac{L}{2};\lambda)$ can be computed again by integrating (A2) for $j = 3$ along the segment $[(0,\frac{L}{2}),(0,-\frac{L}{2})]$. It yields

$$\Psi_3\left(0,-\frac{L}{2};\lambda\right) = -\frac{1}{2}\int_{-(L/2)}^{L/2} e^{-\omega[z'+(L/2)]}\left[\imath\theta_{z'}(0,z') - \frac{\imath\Lambda\theta(0,z')}{\lambda} + \int_0^{+\infty}\theta(\xi,z')d\xi - \omega(\lambda)\int_0^{+\infty}\theta_{z'}(\xi,z')d\xi\right]dz'. \tag{A10}$$

Integrating by parts the last double integral,

$$\frac{1}{2}\int_{-(L/2)}^{L/2} e^{-\omega(\lambda)[z'+(L/2)]}\omega(\lambda)\int_0^{+\infty}\theta_{z'}(\xi,z')d\xi\,dz' = \frac{\omega}{2}\left[e^{-\omega L}\int_0^{\infty}\theta\left(\xi,\frac{L}{2}\right)d\xi - \int_0^{\infty}\theta\left(\xi,-\frac{L}{2}\right)d\xi\right] + \frac{\omega^2}{2}\int_{-(L/2)}^{L/2} e^{-\omega(\lambda)[z'+(L/2)]}\int_0^{\infty}\theta(\xi,z')d\xi\,dz', \tag{A11}$$

the previous expression reads

$$\Psi_3\left(0,-\frac{L}{2};\lambda\right)=\frac{1}{2}\int_{-(L/2)}^{L/2}e^{-\omega[z'+(L/2)]}\left[-\imath\theta_{z'}(0,z')+\frac{\imath\Lambda\theta(0,z')}{\lambda}-\Omega^2\int_0^{+\infty}\theta(\xi,z')d\xi\right]dz'$$
$$+\frac{\omega}{2}\left[e^{-\omega L}\int_0^{+\infty}\theta\left(\xi,\frac{L}{2}\right)d\xi-\int_0^{+\infty}\theta\left(\xi,-\frac{L}{2}\right)d\xi\right]dz' \tag{A12}$$

for any $\lambda\in\mathbb{C}$.

Although the constants introduced in (A4)–(A6) contain information about the boundary value problem, they still require unknown data. Hence, further manipulations are needed in order to suppress them.

Turning again our attention to the original problem (32), Eqs. (A9) and (A12) become

$$\Psi_1\left(0,\frac{L}{2};\lambda\right)=\frac{\Omega(\lambda)}{2}\int_0^{\infty}e^{-\Omega x'}\int_{x'}^{+\infty}\theta_z\left(\xi,\frac{L}{2}\right)d\xi\,dx', \tag{A13}$$

$$\Psi_3\left(0,-\frac{L}{2};\lambda\right)=\frac{i\pi[1-e^{-\omega(\lambda)L}]}{\lambda^2+1}-\frac{\Omega^2}{2}\int_{-(L/2)}^{L/2}e^{-\omega[z'+(L/2)]}\int_0^{+\infty}\theta(\xi,z')d\xi\,dz', \tag{A14}$$

both still containing unknown functions.

To have more restrictions on them, we look at their symmetries. First, the z-mirror symmetry,

$$\theta(x,-z)=\theta(x,z) \tag{A15}$$

implies

$$\Psi_1\left(0,\frac{L}{2};\lambda\right)=-\Psi_1\left(0,-\frac{L}{2};\lambda\right) \tag{A16}$$

for (A13), which, used in the global symmetry (A7), leads to

$$\Psi_3\left(0,-\frac{L}{2};\lambda\right)=(e^{-\omega L}+1)\Psi_1\left(0,-\frac{L}{2};\lambda\right). \tag{A17}$$

Now, since $\Psi_1(0,-\frac{L}{2};\lambda)$ depends on λ only through $\Omega(\lambda)$, it will enjoy the same inversion symmetry $\lambda\to-\frac{1}{\lambda}$, namely,

$$\Psi_1\left(0,-\frac{L}{2};-\frac{1}{\lambda}\right)=\Psi_1\left(0,-\frac{L}{2};\lambda\right). \tag{A18}$$

On the other hand, $\Psi_3(0,-\frac{L}{2};\lambda)$ in (A14) depends on λ through both ω and Ω^2, thus, being invariant under $\lambda\to\frac{1}{\lambda}$,

$$\Psi_3\left(0,-\frac{L}{2};\lambda\right)-\frac{\imath\pi(1-e^{-\omega(\lambda)L})}{\lambda^2+1}=\Psi_3\left(0,-\frac{L}{2};\frac{1}{\lambda}\right)$$
$$-\frac{\imath\pi\lambda^2(1-e^{-\omega(\lambda)L})}{\lambda^2+1}. \tag{A19}$$

Applying the transformation $\lambda\to\frac{1}{\lambda}$ into (A17) and (A18), substituting into (A19), and rearranging the various terms, we are led to the equation,

$$\Psi_1\left(0,-\frac{L}{2};\lambda\right)-\Psi_1\left(0,-\frac{L}{2};-\lambda\right)=G_1(\lambda), \tag{A20}$$

which, because of the convergence region for Ψ_1, only makes sense for $\lambda\in\mathbb{R}$ with

$$G_1(\lambda)=\frac{\imath\pi}{4}\frac{1-\lambda^2}{1+\lambda^2}\frac{e^{\omega(\lambda)L}-1}{e^{\omega(\lambda)L}+1}. \tag{A21}$$

Analogously, using again (A17) and the above symmetries, one obtains

$$\Psi_3\left(0,-\frac{L}{2};\lambda\right)-(e^{-\omega L}+1)\Psi_1\left(0,-\frac{L}{2};-\lambda\right)=G_2(\lambda), \tag{A22}$$

which holds on $\lambda\in\mathbb{C}^-$ and where

$$G_2(\lambda)=\frac{\imath\pi}{4}\frac{1-\lambda^2}{1+\lambda^2}(1-e^{-\omega(\lambda)L}). \tag{A23}$$

Both G_1 and G_2 now only encode information about the boundary conditions, but in order to use them, one has to suitably modify the relations (A4)–(A6). Precisely, defining the new $\tilde{\Psi}_j$ [coherently with the definition (A2)],

$$\begin{aligned}\Psi_1&=\tilde{\Psi}_1\lambda\in\mathbb{C}^+,\\ \Psi_2&=\tilde{\Psi}_2-e^{\Omega x+\omega[z+(L/2)]}\Psi_1\left(0,-\frac{L}{2};-\lambda\right)\lambda\in\mathbb{C}^{\mathrm{III}},\\ \Psi_3&=\tilde{\Psi}_3+e^{\Omega x+\omega[z-(L/2)]}\Psi_1\left(0,-\frac{L}{2};-\lambda\right)\lambda\in\mathbb{C}^{\mathrm{IV}},\end{aligned} \tag{A24}$$

the relations (A4)–(A6) read

$$\begin{aligned}\tilde{\Psi}_3-\tilde{\Psi}_1&=e^{\Omega x+\omega z}e^{-\omega(L/2)}G_1(\lambda),\quad \lambda\in\mathbb{R}^+,\\ \tilde{\Psi}_3-\tilde{\Psi}_2&=e^{\Omega x+\omega z}e^{\omega(L/2)}G_2(\lambda),\quad \lambda\in\imath\mathbb{R}^-,\\ \tilde{\Psi}_1-\tilde{\Psi}_2&=e^{\Omega x+\omega z}e^{\omega(L/2)}G_1(\lambda),\quad \lambda\in\mathbb{R}^-.\end{aligned} \tag{A25}$$

The system (A25) is a Riemann-Hilbert problem defined on three branches where the jumps are completely known

functions. Furthermore, going back to (A8) and estimating its asymptotic behavior for $\lambda \to \infty$, one obtains a reference value for $\tilde{\Psi}_1$,

$$\tilde{\Psi}_1(x,z;\lambda) = \frac{1}{2}\int_x^{+\infty} \theta_z(\xi,z)d\xi + O\left(\frac{1}{\lambda}\right). \tag{A26}$$

Thus, from the jump conditions (A25) and the asymptotic value (A26), $\tilde{\Psi}_1$ is given by

$$\begin{aligned} 2\pi\imath\left[\tilde{\Psi}_1(x,z;\lambda) - \frac{1}{2}\int_x^{+\infty}\theta_z(\xi,z)d\xi\right] &= \int_{-\infty}^{0} e^{\Omega(\lambda')x+\omega(\lambda')[z+(L/2)]}\frac{G_1(\lambda')}{\lambda'-\lambda}d\lambda' \\ &+ \int_{\infty}^{0} e^{\Omega(\lambda')x+\omega(\lambda')[z-(L/2)]}\frac{G_1(\lambda')}{\lambda'-\lambda}d\lambda' \\ &+ \int_{0}^{-\imath\infty} e^{\Omega(\lambda')x+\omega(\lambda')[z+(L/2)]}\frac{G_2(\lambda')}{\lambda'-\lambda}d\lambda', \end{aligned} \tag{A27}$$

which holds for $\lambda \in \mathbb{C}^+$. On the other hand, from the component dx of the linear problem (A2) or from the solution (A8) in the limit $\lambda \to 0$, one obtains

$$\theta = -\imath \lim_{\lambda\to 0}\left[\tilde{\Psi}_1(x,z;\lambda) - \frac{1}{2}\int_x^{+\infty}\theta_z(\xi,z)d\xi\right]. \tag{A28}$$

Comparing the last two relations, one obtains the solution of the modified Helmholtz BVP (32) by the final formula,

$$\begin{aligned} \theta_+(x,z) = \frac{-1}{2\pi}\Bigg[&\int_{-\infty}^{0} e^{\Omega(\lambda)x+\omega(\lambda)[z+(L/2)]}G_1(\lambda)\frac{d\lambda}{\lambda} \\ &+ \int_{\infty}^{0} e^{\Omega(\lambda)x+\omega(\lambda)[z-(L/2)]}G_1(\lambda)\frac{d\lambda}{\lambda} \\ &+ \int_{0}^{-\imath\infty} e^{\Omega(\lambda)x+\omega(\lambda)[z+(L/2)]}G_2(\lambda)\frac{d\lambda}{\lambda}\Bigg]. \end{aligned} \tag{A29}$$

One can check that the solution (A29) certainly satisfies the boundary conditions in (32).

Now, if one sets $z = -\frac{L}{2} + \epsilon$ with $0 < \epsilon < \frac{L}{2}$, it can be verified that the integrands in (36) are bounded and analytic functions in C^{IV}. Thus, performing as above, the change in variable $\lambda \to -\frac{1}{\lambda}$ on the first term, we are led to an integrand split into an analytic part plus a meromorphic contribution $-\imath\frac{e^{\Omega(\lambda)x}}{2\lambda}\frac{(1-\lambda^2)}{(1+\lambda^2)}\frac{(1-e^{-\omega(\lambda)\epsilon})}{(e^{L\omega(\lambda)}+1)}$, containing all poles in the family $P_G^- = \{\lambda_\in P_G,\ \Im\lambda_n < 0\}$. Thus, the solution is given in terms of the series of its residues. Noting that

$$\begin{aligned} \lambda_{-(n+1)} &= -\lambda_n - 2\imath\sqrt{1+(2n+1)^2\pi^2}, \\ \Omega(\lambda_{-(n+1)}) &= \Omega(\lambda_n), \\ \omega(\lambda_{-(n+1)}) &= -\omega(\lambda_n), \\ \mathrm{Res}(e^{L\omega(\lambda)}+1)^{-1}|_{\lambda_{-(n+1)}} &= -\mathrm{Res}(e^{L\omega(\lambda)}+1)^{-1}|_{\lambda_n} - 2, \end{aligned} \tag{A30}$$

one can first sum up the contributions coming from the poles λ_n and $\lambda_{-(n+1)}$, collecting the exponential x dependence and the trigonometric z dependence. This manipulation leads directly to the formula (34).

[1] R. D. Kamien and J. V. Selinger, J. Phys.: Condens. Matter **13**, R1 (2001).

[2] P. Oswald and P. Pieranski, *Nematic and Cholesteric Liquid Crystals: Concepts and Physical Properties Illustrated by Experiments* (CRC, Boca Raton, FL, 2005).

[3] J. Baudry, S. Pirkl, and P. Oswald, Phys. Rev. E **57**, 3038 (1998).

[4] J. Baudry, S. Pirkl, and P. Oswald, Phys. Rev. E **59**, 5562 (1999).

[5] P. Oswald, J. Baudry, and S. Pirkl, Phys. Rep. **337**, 67 (2000).

[6] S. Pirkl and P. Oswald, Liq. Cryst. **28**, 299 (2001).

[7] I. I. Smalyukh, B. I. Senyuk, P. Palffy-Muhoray, O. D. Lavrentovich, H. Huang, E. C. Gartland, V. H. Bodnar, T. Kosa, and B. Taheri, Phys. Rev. E **72**, 061707 (2005).

[8] P. Oswald and A. Dequidt, Phys. Rev. E **77**, 051706 (2008).

[9] T. Akahane and T. Tako, Jpn. J. Appl. Phys. **15**, 1559 (1976).

[10] V. G. Bhide, S. C. Jain, and S. Chandra, J. Appl. Phys. **48**, 3349 (1977).

[11] N. Nawa and K. Nakamura, Jpn. J. Appl. Phys. **17**, 219 (1978).

[12] B. Kerllenevich and A. Coche, Mol. Cryst. Liq. Cryst. **68**, 47 (1981).

[13] T. H. R. Skyrme, Nucl. Phys. **31**, 556 (1962).

[14] P. J. Ackerman, R. P. Trivedi, B. Senyuk, J. van de Lagemaat, and I. I. Smalyukh, Phys. Rev. E **90**, 012505 (2014).

[15] P. J. Ackerman, Z. Qi, and I. I. Smalyukh, Phys. Rev. E **86**, 021703 (2012).

[16] P. J. Ackerman, Z. Qi, Y. Lin, C. W. Twombly, M. J. Laviada, Y. Lansac, and I. I. Smalyukh, Sci. Rep. **2**, 414 (2012).

[17] M. B. Pandey, T. Porenta, J. Brewer, A. Burkart, S. Čopar, S. Žumer, and I. I. Smalyukh, Phys. Rev. E **89**, 060502(R) (2014).

[18] J. I. Fukuda and S. Žumer, Phys. Rev. Lett. **104**, 017801 (2010).

[19] G. De Matteis, L. Martina, and V. Turco, Theor. Math. Phys. **196**, 1150 (2018).

[20] I. I. Smalyukh, Y. Lansac, N. A. Clark, and R. P. Trivedi, Nature Mater. **9**, 139 (2010).

[21] P. J. Ackerman, J. van de Lagemaat, and I. I. Smalyukh, Nat. Commun. **6**, 6012 (2015).

[22] J. Fukuda and S. Žumer, Nat. Commun. **2**, 246 (2011).

[23] J. Eun, S. J. Kim, and J. Jeong, Phys. Rev. E **100**, 012702 (2019).

[24] A. N. Bogdanov and A. A. Shestakov, J. Exp. Theor. Phys. **86**, 911 (1998).

[25] A. N. Bogdanov, U. K. Rößler, and A. A. Shestakov, Phys. Rev. E **67**, 016602 (2003).

[26] A. O. Leonov, I. E. Dragunov, U. K. Rößler, and A. N. Bogdanov, Phys. Rev. E **90**, 042502 (2014).

[27] I. W. Stewart, *The Static and Dynamic Continuum Theory of Liquid Crystals* (Taylor & Francis, London, 2004).
[28] S. Afghah and J. V. Selinger, Phys. Rev. E **96**, 012708 (2017).
[29] P. De Gennes and J. Prost, *The Physics of Liquid Crystals* (Clarendon, Oxford, 1993).
[30] G. De Matteis, D. Delle Side, L. Martina, and V. Turco, Phys. Rev. E **98**, 042702 (2018).
[31] A. B. Borisov and V. V. Kiselev, Inverse Problems **5**, 959 (1989).
[32] J. C. Lee, D. W. Allender, and V. D. Neff, Mol. Cryst. Liq. Cryst. **210**, 11 (1992).
[33] V. K. Andreev, O. V. Kaptsov, V. V. Pukhnachov, and A. A. Rodionov, *Applications of Group-Theoretical Methods in Hydrodynamics*, (Kluwer Academic, Dordrecht, 1998).
[34] S. V. Burylov and A. N. Zakhlevnykh, Eur. Phys. J. E **39**, 65 (2016).
[35] C. Rogers and W. K. Schief, *Bäcklund and Darboux Transformations* (Cambridge University Press, Cambridge, UK, 2002), p. 30.
[36] M. J. Ablowitz, D. J. Kaup, A. C. Newell, and H. Segur, Stud. Appl. Math. **53**, 249 (1974).
[37] A. S. Fokas, J. Lenells, and B. Pelloni, J. Nonlin. Sci. **23**, 241 (2013).
[38] A. S. Fokas, *A Unified Approach to Boundary Value Problems* (SIAM, Philadelphia, 2008).
[39] P. M. Morse and H. Feshbach, *Methods of Theoretical Physics* (McGraw-Hill, New York, 1953).
[40] Y. Antipov and A. S. Fokas, Math. Proc. Cambridge Philos. Soc. **138**, 339 (2005).
[41] W. H. Press, S. A. Teukolsky, W. T. Vetterling, and B. P. Flannery, *Numerical Recipes*, 3rd ed. (Cambridge University Press, Cambridge, UK, 2007).
[42] R. J. LeVeque, *Finite Difference Methods for Ordinary and Partial Differential Equations: Steady-State and Time-Dependent Problems* (Society for Industrial and Applied Mathematics, Philadelphia, 2007).
[43] MATLAB is a registered trademark of The MathWorks, Inc., http://www.mathworks.com.
[44] P. J. Kedney and I. W. Stewart, Lett. Math. Phys. **31**, 261 (1994).
[45] DLMF-NIST, https://dlmf.nist.gov/4.13.
[46] W. J. A. Goosens, J. de Phys. France **43**, 1469 (1982).
[47] T. J. Scheffer, Phys. Rev. A **5**, 1327 (1972).
[48] M. J. Press and A. S. Arrott, Mol. Cryst. Liq. Cryst. **37**(1), 81 (1976).
[49] P. Ribiere and P. Oswald, J. Phys. France **51**, 1703 (1990).
[50] M. J. Ablowitz and P. A. Clarkson, *Solitons, Nonlinear Evolution Equations and Inverse Scattering* (Cambridge University Press, Cambridge, UK, 1991), Chap. 3.
[51] A. C. L. Ashton, A. S. Fokas, Elliptic boundary value problems in convex polygons with low regularity boundary data via the unified method, arXiv:1301.1490.